A New Active Neutron Multiplicity Measurement Device for Uranium Assay Utilizing a Portable D-D Neutron Generator*

Hao-Ran Zhang,[1,2,3] Yan Zhang,[1,2,†] Chi Liu,[1,2] Wen-Xing Hu,[1,2] Xuan-Di Hu,[1,2,3] Xian-Pei Ou,[1,2] Jin-Hui Qu,[1,2] Ren-Bo Wang,[1,2,4] and Bin Tang[1,2]

[1]*National Key Laboratory of Uranium Resources Exploration-Mining and Nuclear Remote Sensing, East China University of Technology, Nanchang 330013, China*
[2]*Jiangxi Province Key Laboratory of Nuclear Physics and Technology, East China University of Technology, Nanchang, 330013, China*
[3]*School of Nuclear Science and Engineering, East China University of Technology, Nanchang 330013, China*
[4]*Pan China Detect Technology Co. Ltd., Nanchang 330013, China*

Ensuring the safeguards and monitoring of enriched uranium is crucial for preventing its illegal theft, destruction, or transfer under arms control. Non-destructive analysis techniques for uranium quantification play a vital role in this effort. The Am-Li source is widely used as an excitation source in Active Uranium Non-destructive Analysis Techniques. However, as acquiring Am-Li becomes increasingly challenging, controllable accelerator-based neutron sources have emerged as a promising alternative due to their superior energy monochromaticity, controlled yield, and on-demand operational capabilities. This study develops an optimized neutron multiplicity measurement system based on a D-D neutron generator, using metallic uranium samples with varying ^{235}U content. Key parameters, including the distance between the neutron generator and a two-layer ^{3}He detector array, ^{3}He tube length, and the material and thickness of the reflector, were optimized via Monte Carlo simulations. The detection efficiency and neutron decay time of the optimized system were evaluated, followed by experimental validation through the quantification of uranium samples with different ^{235}U enrichments and masses. The results indicate that for highly enriched uranium (^{235}U enrichment >50%), the *M-C* coupling curve yielded a measurement relative deviation of less than 10%, while for other enrichment levels, deviations remained within 100 g. Furthermore, by analyzing fission neutron detection efficiency (ϵ_f) and spatial fission rate variations within the sample chamber, a correction factor (k) was introduced using partial least squares regression to account for sample geometry, density, and ^{235}U abundance, reducing the average relative deviation from 20.67% to 8.18%. This research provides a foundation for further development and experimental validation of neutron multiplicity measurement devices utilizing D-D neutron generators.

Keywords: Neutron Multiplicity, Portable D-D Neutron Generator, Enriched Uranium, Partial Least Squares Regression

I. INTRODUCTION

Uranium resources, as a dual-use strategic asset[1], are pivotal to both nuclear energy and nuclear weapons. Significant progress has been made in nuclear disarmament over recent years. However, with the escalation of international tensions, the smuggling and illicit transfer of uranium materials have become major threats to public safety[2]. As a result, strengthening oversight and control of nuclear materials[3, 4], mitigating nuclear weapon proliferation risks, and ensuring global security have become critical objectives in international nuclear security and safeguards.[5–11]

Within uranium materials, the characteristic gamma-rays of ^{235}U exhibit limited penetration capabilities[13]. Traditional gamma-ray analysis techniques[14–17] are insufficient for determining the mass of ^{235}U in bulk uranium items, such as canned oxides, fuel pellets, and fuel assemblies. Therefore, neutron interrogation methods, including active neutron interrogation[18], active neutron multiplicity measurement[19], prompt neutron measurement, and delayed neutron measurement[15, 20–22], must be employed.

In the context of international safeguards applications, commonly used active neutron systems include the Active Well Coincidence Counter (AWCC)[12], the Uranium Neutron Collar (UNCL), and the ^{252}Cf-Shuffler. These systems rely on neutron interrogation with isotopic neutron sources, such as ^{252}Cf[23, 24] or Am-Li, to precisely measure uranium-containing objects with high quality and density, which are difficult to analyze accurately using gamma-ray techniques. However, the isotopic neutron sources required by active measurement systems like AWCC and UNCL, especially Am-Li sources, are no longer produced by many countries[25]. The use of Am-Be sources as substitutes is impractical due to their average energy significantly exceeding the induced fission threshold of ^{238}U. The ^{252}Cf-Shuffler system, which relies on the high neutron flux from ^{252}Cf sources, remains viable but presents substantial challenges due to the short half-life of ^{252}Cf and significant shielding requirements. As a result, routine operational use has become prohibitively expensive, necessitating replacement every five to seven years.

The absence of suitable alternative neutron sources represents a significant challenge in the nuclear security and safeguards of uranium materials. Accelerator-driven neutron sources, distinguished by their superior energy monochro-

* Supported by the National Natural Science Foundation of China (NO. 42374226), Jiangxi Provincial Natural Science Foundation of China (NO. 20232BAB201043, 20232BCJ23006 and gpyc20240073), National Key Laboratory of Uranium Resource Exploration Mining and Nuclear Remote Sensing(ECUT) of China (2024QZ-TD-09) and Young Talent Support Project (ECUT) of China (DHTJBJ202402).

† Corresponding author, yanzhang@ecut.edu.cn.

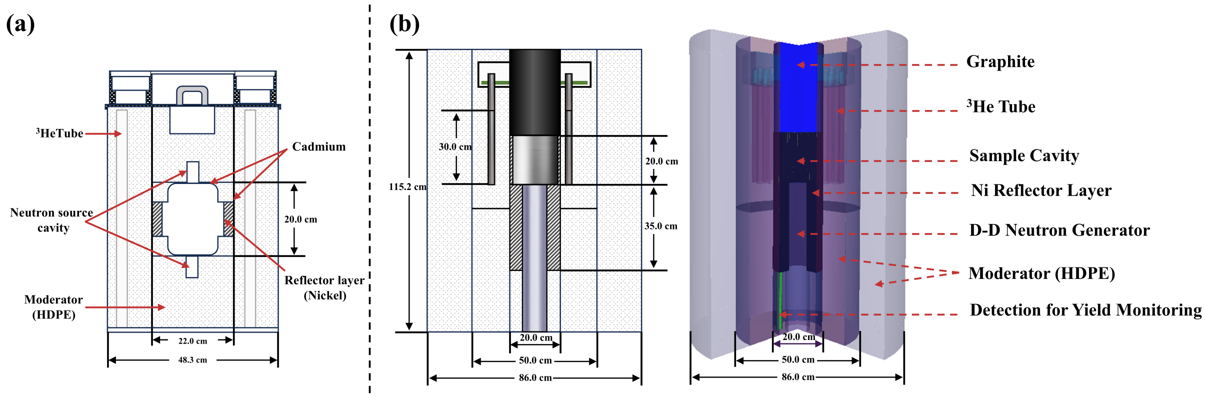

Fig. 1. Structural diagram of Active Well Coincidence Counter. (a):AWCC[12] ;(b):The New Neutron Multiplicity Device Based on Portable D-D Neutron

maticity, controllable yield, and on-demand operation, have emerged as the preferred alternatives to isotopic neutron sources[26, 27]. This study employs Monte Carlo (MC) simulation[28, 29] software to design and optimize an active neutron multiplicity device based on a portable D-D neutron generator [30], replacing traditional interrogation sources. Simulations conducted on various uranium metal components with differing ^{235}U enrichments demonstrate the feasibility of the device design and validate the accuracy of uranium quantification.

II. DEVICES AND PRINCIPLES FOR URANIUM MASS CALCULATION

A. Principle of Active Neutron Multiplicity Uranium Mass Calculation

The active multiplicity measurement method involves analyzing the neutron leakage multiplication M and the induced fission rate F of a sample by utilizing the single counting rate (S), double counting rate (D), and triple counting rate (T). Eqs. (1), (2), and (3) describe the relationships between the multiplicity count rates S, D, T and the parameters M, F. By simultaneously solving Eq.(2) and Eq.(3), the values of M and F can be determined, enabling the calculation of the total mass of ^{235}U in the sample using Eq.(4) [2, 31–33].

$$S = S_0 + B + S_S + FM\varepsilon_f v_{s1} \tag{1}$$

$$D = \frac{F\varepsilon_f^2 f_d v_{s2} M^2}{2}\left[1 + \frac{(M-1)v_{s1}v_{i2}}{v_{s2}\,(v_{i1}-1)}\right] \tag{2}$$

$$T = \frac{F{\varepsilon_f}^3 f_t v_{s3} M^3}{6}\left[\begin{array}{c} 1 + \frac{(M-1)(3v_{s2}v_{i2}+v_{s1}v_{i3})}{v_{s3}(v_{i1}-1)} \\ + \frac{(M-1)3v_{s1}{v_{i2}}^2}{v_{s3}(v_{i1}-1)^2} \end{array}\right] \tag{3}$$

Where S_0 represents the counting rate of the excitation source; B denotes the background counting rate; Ss accounts for the scattering of the source neutrons by the sample; F is the sample-induced induced fission rate, measured in counts per second s^{-1}; M is the neutron leakage multiplication; ϵ_f represents the detection efficiency for induced fission neutrons; v_{s1}, v_{s2}, and v_{s3} correspond to the first, second, and third reduced moments of uranium fission induced by the excitation source, respectively; v_{i1}, v_{i2}, and v_{i3} denote the first, second, and third reduced moments of uranium fission induced by secondary fission neutrons; while f_d is the double gate factor and f_t is the triple gate factor.

$$m_{235} = \frac{F}{CY} \tag{4}$$

In Eq.(4), C represents the coupling coefficient of the apparatus, as shown in Eq.(5), which is determined from the calibration with standard samples; m_{235} denotes the total mass of ^{235}U in the sample, and Y is the neutron yield of the neutron source.

$$C = a - \frac{b(M-1)}{1+c(M-1)} \tag{5}$$

where a, b, and c are calibration constants obtained through data fitting.

B. Structure of Active Neutron Multiplicity Device

The structural configurations of active neutron multiplicity devices vary depending on the neutron detectors employed [34, 35]. These devices are typically composed of multiple ^{3}He neutron detectors (^{3}He tubes) [36, 37] or boron-coated straw detectors (boron-coated straw tubes) [38, 39]. However, they are limited to detecting neutrons within the thermal or epithermal energy range. To facilitate this, the devices incorporate moderation layers made of materials such as high-density polyethylene (HDPE), paraffin, water, and others[40],

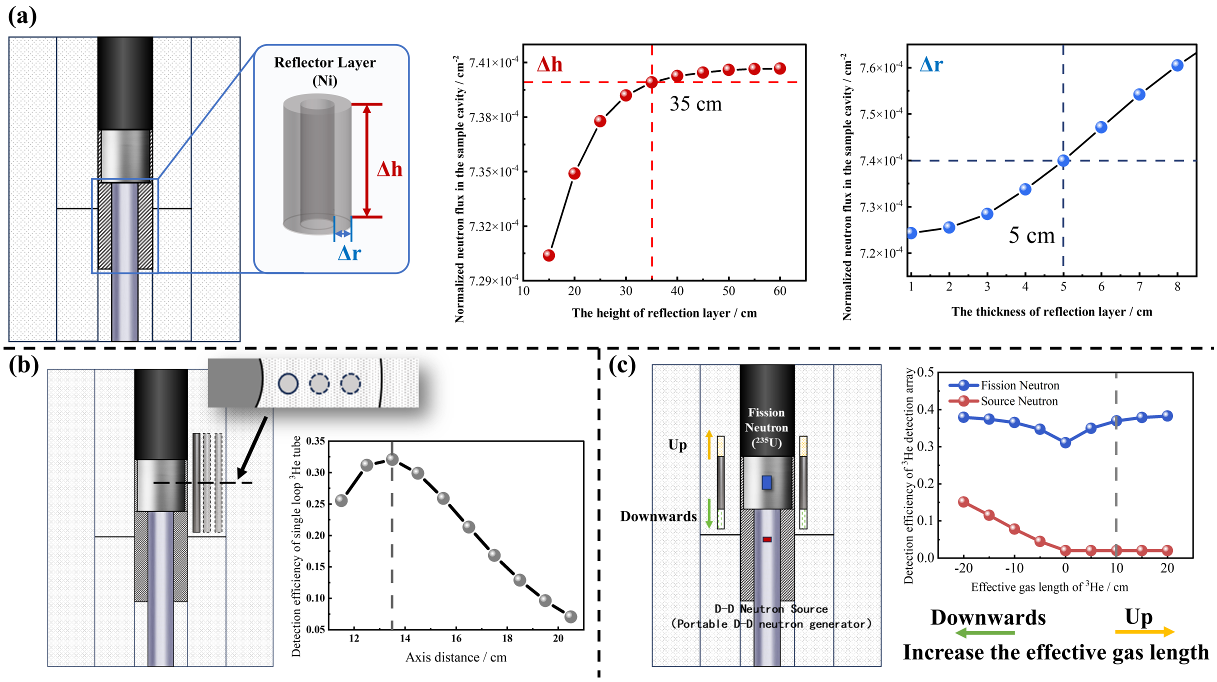

Fig. 2. Optimization simulation of device structure. (a): Nickel reflector layer; (b): Detection array composed of ^{3}He tubes ; (c): The length of ^{3}He tubes' effective gas;

ensuring effective neutron capture by the detectors and the generation of pulse signals. Factors such as the number and layout of detectors, along with additional structural characteristics, collectively influence the detection efficiency of these devices, which typically ranges from 20% to 60%[41–43].

The classic active device depicted in Fig. 1 (a) is the AWCC [12], produced by Canberra, USA. The main body of the device is constructed from high-density polyethylene (HDPE) and features a cylindrical structure approximately 50 cm in diameter and 70 cm in height. The measurement cavity has dimensions of Φ22.9 cm × 20.6 cm. Surrounding the sample cavity are two rings, each containing 21 ^{3}He tubes, for a total of 42 ^{3}He tubes arranged in an array. These detectors are encased in HDPE and are primarily designed to detect thermal neutrons within the detection system.

Both the upper and lower parts of the sample chamber are equipped with neutron source chambers specifically designed for placing Am Li sources. The device's detection efficiency, calibrated using a ^{252}Cf neutron source, is measured at 26%, with a neutron die-away time of 50 μs.

When measuring uranium samples, the Am-Li sources placed in the neutron source cavity emit neutrons to induce ^{235}U fission in the sample, producing induced fission neutrons. The ^{235}U mass is calculated using Eqs. (1) - (4) based on the multiplicity counting rate recorded by the ^{3}He tube. However, before this calculation, standard samples are required to calibrate and fit Eq. (5).

C. The Neutron Multiplicity Device Based on Portable D-D Neutron Generator

The new device replaces the original two isotopic excitation sources with a single portable D-D neutron generator, positioned beneath the sample cavity (Fig. 1 (b)). Neutron emission is controlled via external programs, significantly reducing daily radiation protection costs. In operation, the generator emits neutrons that induce fission in the sample, and the resulting mass of ^{235}U is determined through detector measurements and software analysis, completing the process.

The device consists of eleven components arranged from top to bottom: electronic circuits[35, 44, 45], graphite plug, inner HDPE moderation body, ^{3}He tube array, sample cavity, portable D-D neutron generator (with neutron source), Ni reflector layer (to enhance neutron flux in the cavity), outer HDPE (for shielding against external neutron interference), cadmium (Cd) layer (to absorb thermal neutrons), and a bottom section of ^{3}He tubes for monitoring the stability of the neutron generator yield, as shown in Fig. 1 (b). Additionally, 1 mm thick Cd layers are placed at the junctions of the sample cavity, outer device layers, and the generator array.

The Cd layers serve two functions: absorbing thermal neutrons returning to the cavity after moderation, thereby reducing secondary fission events, and absorbing neutrons that are moderated but not detected by the array or leaked directly from the generator, providing additional radiation shielding. The device is cylindrical, 115 cm tall, and 86 cm in diameter.

III. DEVICE OPTIMIZATION AND CALIBRATION SIMULATION

After finalizing the core structure of the device (Fig. 1 (b)), further optimization of component specifications and configuration is required to enhance the detection array's efficiency and neutron source utilization. The quantity, diameter, tube length, and arrangement of ^{3}He neutron detectors significantly affect detection efficiency, directly influencing the device's performance. Additionally, since the portable D-D neutron generator emits neutrons across a 4π solid angle, reflector layers are crucial to maximize neutron utilization.

Due to the device's complexity, optimizing its design through theoretical calculations is challenging. Therefore, this study employs Monte Carlo (MC) software to model the device and simulate the layout of the portable D-D neutron generator, detection array, reflector layers, and other components. This approach aims to further optimize detection efficiency and measurement accuracy, enhancing the device's practical applicability.

A. Nickel reflector layer

The reflector layer is configured as a hollow cylinder, with an inner diameter set to 10.2 cm based on the selected neutron generator model. The outer diameter and height will be further determined according to design specifications.

Two MC simulation models, shown in Fig.2 (a).

Based on the simulation curve Δh shown in Fig. 2 (a), with the reflector layer thickness (outer diameter) held constant, the neutron flux within the sample cavity remains relatively unchanged after increasing the reflector height to 35 cm. Therefore, a reflector layer height of 35 cm is selected.

With the reflector layer height fixed at 35 cm, the outer diameter is increased, as shown by Δr in Fig.2 (a), increasing the reflector thickness Δr enhances the neutron flux in the cavity, thereby improving neutron utilization efficiency. However, considering material constraints, particularly for ^{3}He tubes, the final selection aligns the reflector thickness with that of the sample cavity, resulting in a hollow cylinder with an outer diameter of 20 cm, inner diameter of 10.2 cm, and height of 35 cm.

At the upper end of the device, graphite is used as the primary material, forming a cylindrical structure with a diameter of 20 cm and a height of 35 cm. Surrounding the sample cavity is a 1 mm-thick cadmium layer, designed to absorb thermal neutrons scattered back into the cavity.

B. Detection array composed of ^{3}He tubes

In the design and optimization of the neutron multiplicity device based on the portable D-D neutron generator, the selection of ^{3}He tubes is critical, as it directly affects response speed, detection efficiency, and cost. Key parameters, including tube length, gas pressure, operating voltage, electrode radius (anode wire, tube wall), and their quantity and distribution, require careful consideration.

To simplify the selection, this study uses ^{3}He tubes with a diameter of 25.4 mm and a gas pressure of 4 atm as the baseline for device design. These specifications were chosen to optimize performance and ensure compatibility with the intended multiplicity measurement application.

The ^{3}He tubes were arranged at axial distances ranging from 11.5 cm to 20.5 cm from the sample cavity's center, corresponding to 1–10 cm from the cavity. Detection efficiency was measured across 21 tubes. To minimize the impact of the effective tube length, each tube was standardized to 50 cm and symmetrically distributed around the cavity's central axis. A point source was placed at the cavity center, with neutron energy spectra tailored to match those verified by M. Devlin et al. using the ENDF/B-VII.1 database[46], specifically for prompt neutrons induced by fast neutrons (2–3 MeV) interacting with ^{235}U[47].

The detection efficiency of the ^{3}He tube array is shown in Fig. 2 (b), with peak efficiency at an axial distance of 13.5 cm. Therefore, the first ring of ^{3}He tubes is positioned 13.5 cm from the cavity center. To avoid cross-talk, a 4 to 5 cm separation between the two detector rings is maintained, with the second ring placed 17.5 cm from the center. The rings are offset to maximize the neutron capture area and enhance detection efficiency.

The optimal effective length of each ^{3}He tube is determined using the simulation model in Fig.2 (c).

From the efficiency curves for different neutron types in Fig.2 (c), increasing the effective gas length to 30 cm results in marginal improvements in fission neutron detection. Therefore, the effective gas length for the ^{3}He tubes was selected to be 30 cm.

C. Simulation calibration of the device

To evaluate the device's performance and support the calibration of design and production parameters, the device was modeled using MC software. Simulation software was then employed to record data on neutron emission, transport, collision, and induced fission processes. This data was organized and analyzed using MATLAB to simulate the pulse time sequences generated by the detector array during actual measurements[37, 48].

The device model was constructed using MC software according to the configuration shown in Fig. 1 (b). In practical applications, a ^{252}Cf source is typically used to calibrate the detector efficiency (ϵ_f) and the neutron die-away time (τ), as described in Eqs. (6) and (7).

$$\varepsilon = \frac{n_{\text{detected}}}{n_{\text{emitted}}} \tag{6}$$

$$D = D_0 \times \left[1 - \exp\left(-\frac{GW}{\tau}\right)\right] \tag{7}$$

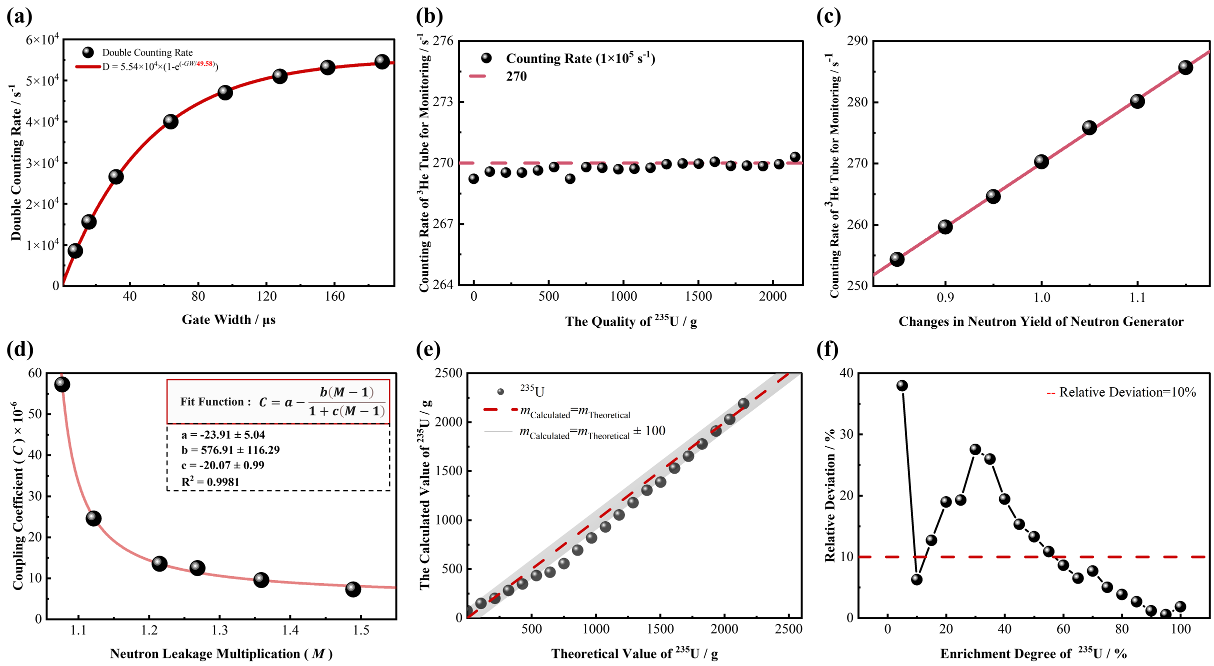

Fig. 3. Simulation and result analysis of sample measurement.(a):The variation of the double counting rate with the width of gate;(b):Changes in counting rate of ^{3}He tube used for bottom monitoring under different ^{235}U masses;(c):Changes in counting rate of ^{3}He tube used for bottom monitoring under different D-D neutron generator yields;(d):M-C coupling curve;(e):^{235}U quantitative result;(f):Relative deviation of ^{235}U quantitative results in samples with different ^{235}U enrichment levels.

Eqs. (6) and (7) present the calibration formulas for detection efficiency (ϵ) and neutron die-away time (τ). In these equations, "n_{detected}" represents the count rate of the device's ^{3}He detection array (in s^{-1}), while "n_{emitted}" is the neutron emission rate from the ^{252}Cf source used during calibration (also in s^{-1}). D denotes the double counting rate, and GW refers to the gate width, measured in microseconds (μs).

The neutron emission rate from the ^{252}Cf source was set at 3.76×10^{5} s^{-1}, with the detector array counting rate at 1.20×10^{5} s^{-1}. Using Eq.(6), the detector array achieved a detection efficiency of approximately 32%. Simulated measurements included a pre-delay time of 3 μs and a long delay time of 2 ms. Various coincidence gate widths—16 μs, 32 μs, 64 μs, 96 μs, 128 μs, 156 μs, and 188 μs—were applied, and the corresponding double counting rates under each gate width were recorded. Curve fitting based on Eq.(7), shown in Fig. 3 (a), indicates a neutron die-away time τ of 49.58 μs, derived from the fitted relationship between gate width and double counting rate.

To assess the impact of uranium mass on the counting rate of the bottom-mounted ^{3}He tube used for background monitoring, 20 metal sphere samples, with ^{235}U masses ranging from 300 g to 2250 g, were placed in the sample chamber. When no sample was present, the counting rate of the bottom ^{3}He tube was recorded as the baseline, corresponding to zero ^{235}U mass. The neutron yield of the portable D-D neutron generator was set at 1×10^{5} s^{-1}. Fig.3 (b) illustrates the variation in the bottom ^{3}He tube counting rate as a function of ^{235}U mass in the sample chamber. Additionally, the counting rate of the bottom ^{3}He tube was recorded with 2250 g of ^{235}U, while varying the neutron yield of the D-D neutron generator from 0.85 to 1.15 times its nominal value, as shown in Fig.3 (c).

As seen in Fig.3 (a), the counting rate of the bottom-mounted ^{3}He tube for background monitoring exhibits minimal variation with ^{235}U mass. With the neutron yield of the portable D-D neutron generator stabilized at 1×10^{5} s^{-1}, the counting rate remains approximately 270 s^{-1}. Variations in the neutron yield of the portable D-D neutron generator correspondingly affect the counting rate of the bottom ^{3}He tube (Fig.3 (b)), demonstrating a linear relationship that satisfies the initial calibration requirements.

IV. SIMULATION AND RESULT ANALYSIS OF SAMPLE MEASUREMENT

A. Simulation of uranium material measurement

The primary distinction between the multiplicity and coincidence measurement methods lies in elevating the coincidence order to triple coincidence. In this quantitative approach, the method surpasses conventional working curve analysis by coupling the double and triple counting rates to determine the sample's neutron leakage multiplication (M)

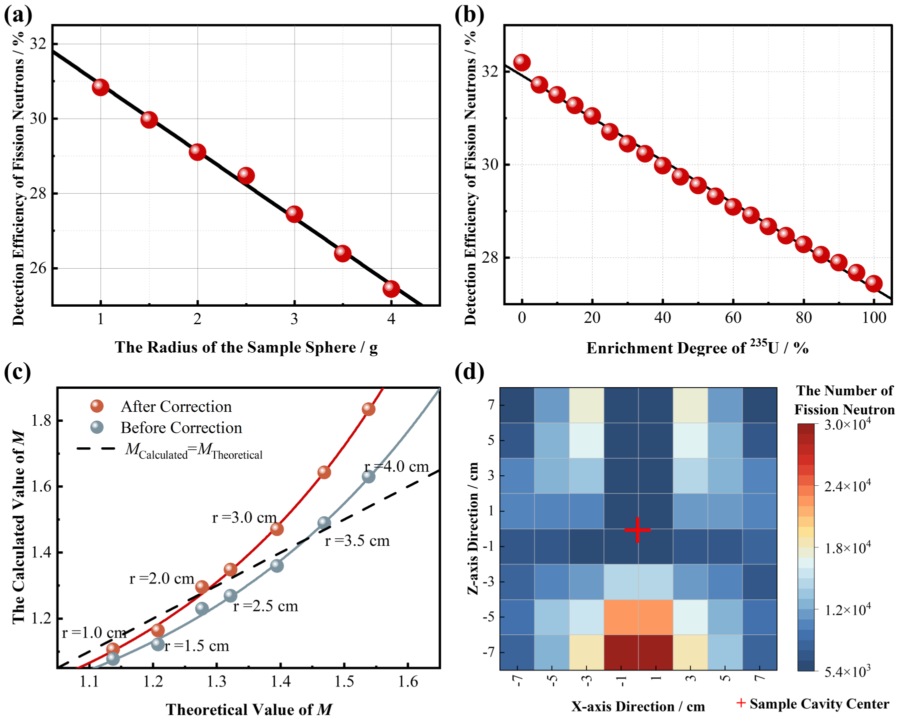

Fig. 4. Quantitative factor analysis of samples.(a): ^{235}U metal with different shapes;(b): ^{235}U metal with the same appearance but different enrichment levels;(c): The theoretical value of neutron leakage multiplication (M) and calculated value after efficiency correction;(d): The number of fission neutrons generated by unit ball samples at different positions in the sample cavity.

and induced fission rate (F) in units of $s^{-1}g^{-1}$. As shown in Eq. (4), prior to sample measurement, it is essential to fit the curve relating neutron leakage multiplication (M) and coupling coefficient (C) based on standard samples, as demonstrated in Eq. (5).

Six metal spheres of ^{235}U, with radii ranging from 1 cm to 3.5 cm at 0.5 cm intervals, were placed at the center of the sample chamber. The neutron yield of the portable D-D neutron generator was set to 1×10^5 s^{-1}, with a single measurement duration of 300 s. Uranium metal spheres of varying ^{235}U enrichment (ranging from 0% to 100%, each with a radius of 3 cm) were used as validation samples.

B. *M*-*C* coupling curve and quantitative analysis

Based on Eq. (5), the fitting analysis is conducted on the relationship between the neutron leakage multiplication (M) and the coupling coefficient (C) of six ^{235}U metallic sphere benchmarks, as shown in Fig. 3(d)[49].

Eq. (8) represents the fitted M-C coupling curve depicted in Fig. 3(d), which is then substituted into equation (4). The relationship between the calculated and actual values of the ^{235}U equivalent mass for different ^{235}U enrichment samples, computed according to equation (4), is illustrated in Fig. 3(e).

$$C = \left(-23.91 - \frac{576.91 \times (M-1)}{1 - 20.07 \times (M-1)}\right) \times 10^{-6} \qquad (8)$$

Fig. 3 (e) shows the relationship between the calculated and theoretical ^{235}U mass in uranium metallic spheres of varying ^{235}U enrichment, using Eq. (8). The red curve represents the line $m_{\text{Calculated}} = m_{\text{Theoretical}}$, indicating that as the calculated values approach the theoretical values—reflecting increased accuracy—more data points align along this line. The black dashed line denotes the region defined by $m_{\text{Calculated}} = m_{\text{Theoretical}} \pm 100$, representing deviations within 100 g from the theoretical values. The distribution of the blue points in Fig. 3(e) suggests that the computational deviations for the uranium metallic sphere samples, derived from the six ^{235}U benchmark samples, are predominantly less than 100 g.

Fig. 3(f) presents the relative deviation statistics of the quantitative results for ^{235}U in samples with varying enrichments. It is evident from the figure that samples with ^{235}U enrichment above 50% exhibit relative deviations of less than 10%. Conversely, as enrichment decreases, the relative errors increase. This can be attributed to the fact that the neutron energy from the portable D-D neutron generator exceeds the induced fission threshold of ^{238}U within the sample[50]. As the mass of ^{238}U increases, more neutrons react with it, as depicted in Fig. 3(f). For enrichments between 10% and 50%, ^{235}U masses are notably underestimated due to neutron re-

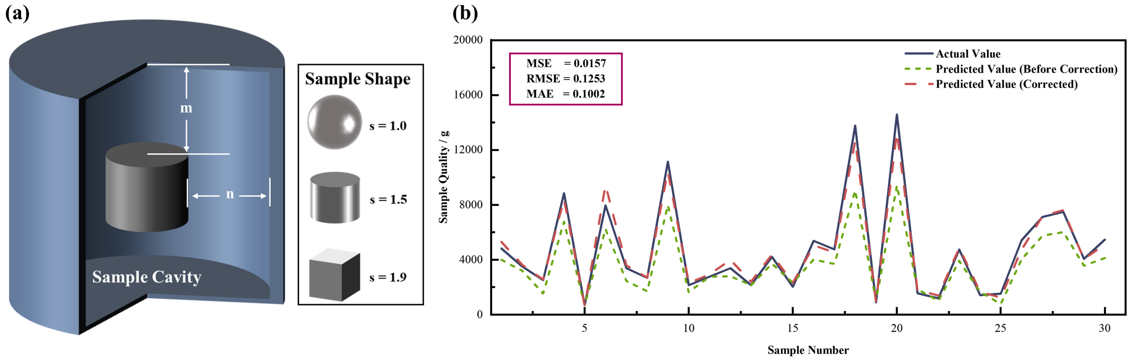

Fig. 5. Parameter interpretation and correction results based on partial least squares regression quality correction method. (a): Coefficient setting situation; (b): Correction result.

actions with ^{238}U[30] or secondary neutron inductions from fission events, which lower the calculated values. As the ^{238}U mass continues to increase, its substantial presence compensates for some of the fission neutrons of ^{235}U, gradually reducing the error.

C. Analysis of the sources of quality calculation errors

The variations in ϵ_f shown in Fig. 4(a) are used to correct the detection efficiency (ϵ_f) for metal spheres of different radii. The neutron leakage multiplication (M), adjusted for efficiency, is then recalculated using Eqs. (2) and (3). The computed values of neutron leakage multiplication (M) for samples of various radii are presented in Fig. 4(c).

After correcting for ϵ_f, the theoretically predicted values of neutron leakage multiplication (M) [51]more closely align with the calculated values for samples with radii smaller than 2.5 cm. However, as the sample radius increases beyond this threshold, the computed neutron leakage multiplication diverges from the theoretical values, particularly for radii greater than 3.0 cm.

In the MC simulation model depicted in Fig. 1(b), a ^{235}U metal sphere with a radius of 1.0 cm was positioned with its center at the origin of the sample chamber. The coordinates along the X and Z axes were varied, and the neutron yield of the portable D-D neutron generator was set to 1×10^5 s^{-1}. The number of fission neutrons emitted from the unit sphere at different locations was recorded, as shown in Fig. 4(d).

Fig. 4(d) reveals significant variation in fission efficiency at different positions within the sample chamber, indicating that fission efficiency is not uniform across the spatial domain. Due to the upward emission of neutrons from the portable D-D neutron generator, the neutron flux is higher at the bottom of the sample chamber, where the sample is placed, resulting in a maximized fission-induced neutron rate in this region. As the unit sphere sample is elevated, the neutron flux decreases due to the larger solid angle subtended by the portable D-D neutron generator and the reduced flux. The surrounding Ni reflector and graphite[52] at the top of the chamber create a neutron flux stabilization region between 4.0 cm and 5.0 cm from the center. In this region, the neutron-induced fission rate remains stable, which is why, as shown in Fig. 4(d), the corrected neutron leakage multiplication (M) closely matches the theoretical values when the sample radius is less than 2.5 cm. Beyond this range, non-uniform fission-induced neutron detection efficiency at different locations leads to deviations between the calculated and theoretical M values.

V. PARTIAL LEAST SQUARES REGRESSION QUALITY CORRECTION METHOD

To address the computational deviations arising from differences between the sample and the reference standard in terms of position within the sample chamber, shape, density, and isotopic abundance, and to simplify the correction process, a correction factor k is introduced in Eq. 4, as shown in Eq. 9:

$$m_{235} = k \times \frac{F_{235}}{CY} \tag{9}$$

The correction factor k is calculated using Eq. 10, where m and n represent the axial and radial distances from the sample surface to the top of the chamber, respectively, when the sample is positioned at the chamber center, as illustrated in Fig. 5(a). These distances, measured in cm, define the spatial position of the sample. The parameter s accounts for the sample shape, calculated using volume formulas for circular, cylindrical, and rectangular shapes when m and n are identical. The variable ρ denotes the sample density (g·cm^{-3}), and f represents the ^{235}U abundance. The coefficients a_i ($i = 1, 2, 3, \ldots$) are regression coefficients. The equation for k is given as:

$$k = a_1 \cdot m + a_2 \cdot n + a_3 \cdot s + a_4 \cdot \rho + a_5 \cdot f + a_6 \tag{10}$$

A total of 300 uranium metal samples with varying shapes, geometries, and isotopic abundances were randomly gener-

ated within the sample chamber. The sample density was randomly set between 16.5 and 19 g·cm^{-3}, ensuring that the mass of ^{235}U remained between 100 and 15,000 g to avoid reaching criticality. Following the mass computation process described in Eqs. 1– 5, the regression terms in Eq. 10 were recorded. Subsequently, 90% of the data was selected for regression fitting of the coefficients a_i using the partial least squares regression (PLSR) algorithm.

The remaining 10% of the data was used for prediction based on the regression matrix. The relationship among the actual sample mass, computed mass, and k-corrected mass is shown in Fig. 5 (b). The black curve represents the actual sample mass, while the green and red curves correspond to the computed mass before and after applying the correction factor k, respectively. By employing the correction factor k, the average relative deviation was reduced from 20.67% to 8.18%, demonstrating good adaptability to variations in sample shape, density, and isotopic abundance.

VI. CONCLUSION

This study designs a neutron multiplicity measurement device based on a D-D neutron source, using Monte Carlo simulations to further optimize the device's performance in terms of the reflector layer and ^{3}He tube layout. The new device has polyethylene as its main body, with a height of 115 cm and a diameter of 86 cm. It is equipped with 43 ^{3}He tubes, 42 of which are evenly distributed in two concentric rings within the polyethylene moderator, while one is positioned at the bottom to monitor the yield of the D-D neutron generator, thus stabilizing the yield.

Using MC simulations, the overall performance of the new device was studied. The device's detection efficiency is 32.00%, and the neutron decay time is 49.58 μs. When the D-D neutron generator's yield is stable at 1×10^5 s^{-1}, the counting rate at the bottom ^{3}He tube remains at 270 s^{-1}. The M-C coupling curve obtained for highly enriched uranium materials enables preliminary quantification of uranium in materials with various ^{235}U enrichments. The deviation between calculated and theoretical mass values is less than 100 g. For samples with more than 50% ^{235}U enrichment, the relative deviation is below 10%. This research lays the foundation for the development and experimental validation of neutron multiplicity measurement devices based on D-D neutron generators.

The study also discusses the sources of the device's quantitative error and corrects the calculation of the neutron multiplication factor M by acquiring the actual fission neutron detection efficiency ϵ_f. Based on the fission behavior of a unit ^{235}U metal sphere in the sample chamber, the new device shows a stable neutron flux region of only 2.5 cm in size at the center of the sample chamber. To further improve measurement precision, additional optimizations to the sample chamber structure or the spatial distribution of fission neutrons are needed.

Lastly, a correction factor k is proposed to address complex sample measurements, along with a method for fitting regression coefficients using the partial least squares regression (PLSR) algorithm. The average relative deviation of the corrected sample mass was reduced from 20.67% to 8.18%. This study, through MC simulations, validates the feasibility and practicality of the D-D neutron source-based multiplicity measurement device for production applications, providing a reference for the design of active neutron multiplicity instruments and uranium quantification methods.

ACKNOWLEDGMENT

The authors would like to thank Pan-China Detect Technology Co. , Ltd. for their support in terms of device parameters and research sites.

AUTHOR CONTRIBUTIONS

All authors contributed to the study conception and design. Material preparation, data collection and analysis were performed by Hao-Ran Zhang, Yan Zhang, Chi Liu, Wen-Xing Hu, Xuan-Di Hu, Xian-Pei Ou, Jin-Hui Qu, Ren-Bo Wang, and Bin Tang. The first draft of the manuscript was written by Hao-Ran Zhang and Yan Zhang, and all authors commented on previous versions of the manuscript. All authors read and approved the final manuscript.

DATA AVAILABILITY STATEMENT

The data that support the findings of this study are openly available in Science Data Bank at https://cstr.cn/31253.11.sciencedb.11259 and https://doi.org/10.57760/sciencedb.11259.

VII. CONFLICT OF INTEREST

The authors declare that they have no competing interests.

VIII. BIBLIOGRAPHY

[1] Y. Zhang, C. Liu, S.L. Liu et al., Prompt fission neutron uranium logging (II): dead-time effect of the neutron time spectrum. Nucl. Sci. Tech. **36**, 19 (2025). doi: https://doi.org/10.1007/s41365-024-01615-x

[2] D. Reilly, N. Ensslin, H. Smith Jr, et al., Passive nondestructive assay of nuclear materials. Nuclear Regulatory Commission,

Washington, DC (1991).

[3] Q.Q. Pan, Q.F. Zhao, L.J. Wang et al., High-resolution neutronics model for 238Pu production in high-flux reactors. Nucl. Sci. Tech. **35**, 88 (2024). doi: https://doi.org/10.1007/s41365-024-01461-x

[4] Z.Y. Yu, Y. Zhang, X.J. Zhang et al., Based on the thickness equivalent basis effect decomposition method of ore separation by multi-energy X-ray transmission technology. Appl. Radiat. Isot. **219**, 111710 (2025). doi: https://doi.org/10.1016/j.apradiso.2025.111710

[5] B. Goddard, Quantitative NDA measurements of advanced reprocessing product materials containing uranium, neptunium, plutonium, and americium. PhD Thesis, Texas A&M University (2013).

[6] H.R. Zhang, Y. Zhang, W.X. Hu et al., Simulation study of uranium content in uranium yellow cake using the active multiplicity method. Nucl. Tech. **47**, 49–57 (2024). doi: https://doi.org/10.11889/j.0253-3219.2024.hjs.47.020202

[7] D. Lao, Y. Zhang, L.F. Huang et al., Microstructure, mechanical and neutron shielding properties of aluminum borate ceramics obtained from alumina and boric acid. J. Aust. Ceram. Soc. **1**, 1–11 (2024). doi: https://doi.org/10.1007/s41779-024-01031-9

[8] Y. Zhang, C.Q. Fu, J. Qiu et al., System optimization study of hybrid K-edge/XRF densitometer for uranium–plutonium solution measurement. Appl. Radiat. Isotopes. **210**, 111367 (2024). doi: https://doi.org/10.1016/j.apradiso.2024.111367

[9] J. Qiu, Y. Zhang, C.Q. Fu et al., Study on photofluorescent uranium ore sorting based on deep learning. Miner. Eng. **206**, 108523 (2024). doi: https://doi.org/10.1016/j.mineng.2023.108523

[10] Y. Zhang, Y.J. Ye, J. Qiu et al., Study on quantitative interpretation of uranium spectral gamma-ray logging based on machine learning algorithm. Nucl. Eng. Tech. (2024). doi: https://doi.org/10.1016/j.net.2024.07.004

[11] F. Jallu, P.-G. Allinei, P. Bernard et al., The use of non-destructive passive neutron measurement methods in dismantling and radioactive waste characterization. In: *Proceedings of the 2011 2nd International Conference on Advancements in Nuclear Instrumentation, Measurement Methods and their Applications*. IEEE (2011). doi: https://doi.org/10.1109/ANIMMA.2011.6172926

[12] T. R. Wenz, H. O. Menlove, G. W. Salton et al., Design and calibration of the AWCC for measuring uranium hexafluoride. Los Alamos National Lab., Los Alamos, NM (United States) (1995).

[13] C. C. Cowles, R. S. Behling, G. R. Imel et al., Effects of correlated and uncorrelated gamma rays on neutron multiplicity counting. IEEE T. Nucl. Sci. **64**, 1865–1870 (2017). doi: https://doi.org/10.1109/TNS.2017.2667407

[14] M.C. Qiu, W.B. Jia, D.Q. Hei et al., Digital stabilization algorithm for the gamma spectra of scintillator detectors in PGNAA. IEEE T. Nucl. Sci. **69**, 113–117 (2021). doi: https://doi.org/10.1109/TNS.2021.3139391

[15] E. Simon, F. Jallu, B. Pérot et al., Fissile mass quantification in radioactive waste packages using photofission delayed gamma rays. In: *Proceedings of the 2016 IEEE Nuclear Science Symposium, Medical Imaging Conference and Room-Temperature Semiconductor Detector Workshop (NSS/MIC/RTSD)*. IEEE (2016). doi: https://doi.org/10.1109/NSSMIC.2016.8069819

[16] Y.C. Yan, M.Z. Liu, X.Y. Li et al., Improved Cohen-Sutherland algorithm for TGS transmission imaging. Nucl. Sci. Tech. **34 (06)**, 206–217 (2023). doi: https://doi.org/10.1007/s41365-023-01238-8

[17] H.H. Ding, F. Gao, C.B. Lu et al., Gamma ray multiplicity of a 240Pu solid sphere simulated by JMCT. Nucl. Sci. Tech. **33**, 53 (2022). doi: https://doi.org/10.1007/s41365-022-01043-9

[18] A. Ndoye, F. Cosset, B. Barelaud et al., Neutron radiation of an electronic sensor using coincidence method for an active dosimeter. Nucl. Instrum. Methods Phys. Res. A **423**, 414–420 (1999). doi: https://doi.org/10.1016/S0168-9002(98)01314-X

[19] M. C. Tweardy, S. McConchie, J. P. Hayward et al., A point kinetics model for estimating neutron multiplication of bare uranium metal in tagged neutron measurements. IEEE T. Nucl. Sci. **64**, 1963–1969 (2017). doi: https://doi.org/10.1109/TNS.2017.2715238

[20] M. Andrews, Delayed neutron & gamma measurements of special nuclear materials, their Monte Carlo simulations, and applications. PhD Thesis, Royal Military College of Canada (2015).

[21] D. Reilly, N. Ensslin, H. Smith, S. Kreiner, Passive nondestructive assay of nuclear materials addendum. **2**, 1–56 (2007).

[22] C. Deyglun, C. Carasco, B. Pérrot et al., Passive and active correlation techniques for the detection of nuclear materials. IEEE T. Nucl. Sci. **61**, 2228–2234 (2014). doi: https://doi.org/10.1109/TNS.2014.2315714

[23] M. A. Schear, S. J. Tobin, Replacing a ^{252}Cf source with a neutron generator in a shuffler—a conceptual design performed with MCNPX. Los Alamos National Laboratory (2009).

[24] B. Goddard, S. Croft, High-fidelity passive neutron multiplicity measurements and simulations of uranium oxide. Nucl. Instrum. Methods Phys. Res. A **712**, 147–156 (2013). doi: https://doi.org/10.1016/j.nima.2013.02.007

[25] R. D. McElroy, S. L. Cleveland, The D-D neutron generator as an alternative to Am(Li) isotopic neutron source in the active well coincidence counter. Oak Ridge National Laboratory (2017).

[26] J. M. Carpenter, The development of compact neutron sources. Nat. Rev. Phys. **1**, 177–179 (2019). doi: https://doi.org/10.1038/s42254-019-0024-8

[27] Y.N. Li, Z. Wei, G.T. Gao et al., Plate spent fuel burnup measurement equipment based on a compact D-D neutron generator. Nucl. Sci. Tech. **36**, 48 (2025). doi: https://doi.org/10.1007/s41365-024-01624-w

[28] X. Wang, L.Y. Zhang, X.M. Shi et al., Optimizations and applications in large-scale scenes of Monte Carlo geometry conversion code CMGC. Nucl. Sci. Tech. **36**, 58 (2025). doi: https://doi.org/10.1007/s41365-024-01634-8

[29] Z.P. Chen, A.K. Sun, J.C. Lei et al., Multi-function and generalized intelligent code-bench based on Monte Carlo method (MagicMC) for nuclear applications. Nucl. Sci. Tech. **36**, 57 (2025). doi: https://doi.org/10.1007/s41365-024-01626-8

[30] E. Edwards, Measurement of krypton fission product yields from 14 MeV neutrons on ^{238}U. University of California, Berkeley (2018).

[31] Y. Zhang, H.R. Zhang, R.B. Wang et al., Passive neutron multiplicity device for ^{240}Pu measurement based on FPGA. Nucl. Sci. Tech. **35**, 162 (2024). doi: https://doi.org/10.1007/s41365-024-01514-1

[32] J. Mattingly, Computation of neutron multiplicity statistics using deterministic transport. IEEE T. Nucl. Sci. **59**, 314–322 (2012). doi: https://doi.org/10.1109/TNS.2012.2185060

[33] M. Bakr, K. Masuda, Y. Takahashi et al., Nondestructive and active interrogation system for special nuclear material: proof of principle and initial results. Nucl. Sci. Tech. **35**, 87 (2024). doi: https://doi.org/10.1007/s41365-024-01458-6

[34] T. H. Shin, A. Di Fulvio, S. D. Clarke et al., Stilbene-based fast neutron multiplicity counter for nuclear safeguards applications. In: *Proceedings of the 2018 IEEE Nuclear Science Symposium and Medical Imaging Conference (NSS/MIC)*. IEEE (2018). doi: https://doi.org/10.1109/NSSMIC.2018.8824630

[35] A. Asghari, S. Dazeley, A. Bernstein, A plutonium mass uncertainty assessment using a Cherenkov-based neutron multiplicity water detector. IEEE Trans. Nucl. Sci. **67**, 2431–2438 (2020). doi: https://doi.org/10.1109/TNS.2020.3027668

[36] J. H. Ely, E. R. Siciliano, A. T. Lintereur et al., Alternatives for helium-3 in multiplicity counters. IEEE T. Nucl. Sci. **60**, 510–514 (2013). doi: https://doi.org/10.1109/TNS.2012.2227123

[37] A. Moore, Modern data acquisition, system design, and analysis techniques and their impact on the physics-based understanding of neutron coincidence counters used for international safeguards. (2019).

[38] J. L. Lacy, A. Athanasiades, L. Sun et al., Boron-coated straws as a replacement for ^{3}He-based neutron detectors. Nucl. Instrum. Methods Phys. Res. A **652**, 359–363 (2011). doi: https://doi.org/10.1016/j.nima.2010.09.011

[39] D. Henzlova, H. O. Menlove, J. B. Marlow, Design and performance of a ^{3}He-free coincidence counter based on parallel plate boron-lined proportional technology. Nucl. Instrum. Methods Phys. Res. A **788**, 188–193 (2015). doi: https://doi.org/10.1016/j.nima.2015.02.050

[40] X.Y. Wang, J.Y. Chen, Q. Zhang, Boron shielding design for neutron and gamma detectors of a pulsed neutron tool. Nucl. Sci. Tech. **36**, 16 (2025). doi: https://doi.org/10.1007/s41365-024-01605-z

[41] E. Aboud, S. Ahn, G.V. Rogachev et al., Modular next generation fast neutron detector for portal monitoring. Nucl. Sci. Tech. **33**, 13 (2022). doi: https://doi.org/10.1007/s41365-022-00990-7

[42] Y.T. Li, W.P. Lin, B.S. Gao et al., Development of a low-background neutron detector array. Nucl. Sci. Tech. **33**, 41 (2022). doi: https://doi.org/10.1007/s41365-022-01030-0

[43] W.L. Pu, Y.L. Ye, J.L. Lou et al., Digital signal acquisition system for complex nuclear reaction experiments. Nucl. Sci. Tech. **35**, 12 (2024). doi: https://doi.org/10.1007/s41365-024-01366-9

[44] M. Ben Mosbah, C. Eleon, C. Passard et al., Performance assessment of amplification and discrimination electronic devices for passive neutron measurements. IEEE Trans. Nucl. Sci. **67**, 662–668 (2020). doi: https://doi.org/10.1109/TNS.2020.2965008

[45] Z.H. Yu, Y. Zhang, H.R. Zhang et al., Optimization study on the compact thermal neutron imaging system based on portable D-T neutron generator. Nucl. Instrum. Meth. A **1069**, 170018 (2024). doi: https://doi.org/10.1016/j.nima.2024.170018

[46] N. Otuka, O. Iwamoto, EXFOR-based simultaneous evaluation of neutron-induced uranium and plutonium fission cross sections for JENDL-5. J. Nucl. Sci. Technol. **59**, 1004–1036 (2022). doi: https://doi.org/10.1080/00223131.2022.2030259

[47] B. Yang, B. Zhong, Q. Xu et al., A Monte-Carlo simulation method for neutron yield and spectrum in (α,n) reaction. Chin. J. Comput. Phys. **38**, 393 (2021). doi: https://doi.org/10.19596/j.cnki.1001-246x.8287

[48] J. K. Halbig, S. C. Bourret, P. R. Collinsworth et al., Recent developments in multiplicity counting hardware at Los Alamos. IEEE T. Nucl. Sci. **39**, 1326–1330 (1992). doi: https://doi.org/10.1109/NSSMIC.1991.259126

[49] W. El-Gammal, W. I. Zidan, E. Elhakim, A proposed semi-empirical method for ^{235}U mass calibration of the active-well neutron coincidence counter. Nucl. Instrum. Methods Phys. Res. A **565**, 731–741 (2006). doi: https://doi.org/10.1016/j.nima.2006.05.171

[50] Y.Y. Ding, Y.B. Nie, Y. Zhang et al., Benchmark experiment on slab 238U with D-T neutrons for validation of evaluated nuclear data. Nucl. Sci. Tech. **35**, 29 (2024). doi: https://doi.org/10.1007/s41365-024-01386-5

[51] C. Lloyd, R. Hadimani, B. Goddard, Time dependent heat transfer of proliferation resistant plutonium. Nucl. Eng. Technol. **51**, 510–517 (2019). doi: https://doi.org/10.1016/j.net.2018.10.024

[52] L. He, J.J. Shen, X.Z. Cai, A thermal–hydraulic model for the graphite-moderated channel-type molten salt reactor. Nucl. Sci. Tech. **36**, 59 (2025). doi: https://doi.org/10.1007/s41365-024-01627-7